Instability of Ultrathin Viscoelastic Freestanding Films

Satya Sekhar[1] and V. Shankar[1, a)]
Department of Chemical Engineering, Indian Institute of Technology, Kanpur 208016, India

The linear stability of freestanding thin films under the influence of attractive van der Waals forces is investigated for three rheological models, viz., Newtonian viscous films, viscoelastic solid films, and Jeffreys viscoelastic liquid films, with the aim of studying the role of rheology on the instability. Thin freestanding viscous films are unconditionally unstable, whereas the shear modulus in thin freestanding solid viscoelastic films governs the onset of instability. Interestingly, elasticity plays a dual role with regard to the stability of freestanding solid and liquid films: while it has a stabilizing influence on the former, it is destabilizing in the latter. Linear stability results of Jeffreys viscoelastic freestanding films are compared with those from supported films in the inertialess limit. The instability of Jeffreys viscoelastic freestanding film is unaffected by the relaxation time, but is enhanced with decrease in the viscosity ratio (μ_r, the ratio of solvent viscosity to total viscosity). The dominant length scale of instability in Jeffreys viscoelastic freestanding film shifts towards shorter wavelengths with decrease in μ_r. For $\mu_r \to 0$, the maximum growth rate remains bounded in a freestanding viscoelastic film in the presence of inertia, but diverges in its absence, similar to supported viscoelastic films. In general, our results show that freestanding thin films exhibit faster dynamics than supported thin films. The mode of deformation of the freestanding film (viz., bending or squeezing) is not imposed a priori in our analysis, and is found to be a squeezing (symmetric) mode with equal amplitudes at the interfaces.

a)Author for correspondence; E-mail: vshankar@iitk.ac.in

I. INTRODUCTION

The instability of thin (<100 nm) films has been extensively studied due to its scientific and technological applications in engineered surfaces[1–3], microfluidics[4,5], dry adhesives[6,7], flotation[8,9], polymer extrusion[10] etc. Most of the theoretical studies on the instability of thin supported polymer films employ the no-slip boundary condition at the solid substrate. However, thin polymer films can exhibit a finite slip[11–14], especially when the substrates are modified using self-assembled monolayers[15] or graftings[16]. Recent experimental studies[10,13] on dewetting of polymer films over lower-energy hydrophobic surfaces suggest that the dynamics of dewetting of such films is more similar to freestanding films. Thus, the actual instability and dynamics of dewetting of thin polymer films on substrates may be expected to lie somewhere in between that of films which obey the no-slip boundary condition and those which satisfy the free-slip condition. Freestanding films having two shear free interfaces are encountered in soap films[17], foams[18] and emulsions[19], and biological membranes[20] etc. The presence of two free interfaces in freestanding films enables two modes of deformation: an in-phase bending/symmetric mode and an out-of-phase squeezing/asymmetric mode. Moreover, when a freestanding film is bounded by identical semi-infinite phases, the configuration is symmetric, while when a freestanding film is surrounded by two different fluids, the configuration is asymmetric[21].

Thin films, owing to their small dimensions, possess excess pressure compared to the bulk of the same material[22]. Interfacial pertrubations get amplified for thin films with negative disjoining pressure leading to spontaneous dewetting eventually leading to film rupture. Thin film instabilities due to intermolecular van der Waals interactions have been extensively studied for supported[23–34] and freestanding[21,35–44] films. Vrij[35] investigated the stability of a thin liquid freestanding film against spontaneous surface corrugations and also explored the kinetics of their diminution and amplification. Ruckenstein and Jain[37] studied the rupture of both supported and freestanding thin liquid films and explored the effect of soluble and insoluble surface active agents on the dynamics of film rupture. They showed that even minute quantities of surface-active impurities induce stronge stabilizing effect, and the time of rupture is several orders of magnitude larger than for a pure liquid. Maldarelli et al.[21] investigated the stability of thin symmetric and asymmetric membranes to short and long wavelength perturbations. Prevost and Gallez[38] derived a nonlinear evolution equation for a thin freestanding film with tangentially immobile surfaces in squeezing mode employing the long-wave scaling of Williams and Davis[23] and showed that nonlinearities significantly accelerate film rupture. Sharma and Ruckenstein[39] developed a theory to predict the critical thickness of rupture of tangentially immobile foam films.

Erneux and Davis[40] used a modified long-wave scaling in order to retain the inertial terms in thin freestanding films and derived coupled nonlinear evolution equations for the film thickness and tangential velocity. De Wit et al.[41] studied the nonlinear evolution of thin freestanding liquid films with insoluble surfactants by numerically solving coupled nonlinear evolution equations for film thickness, tangential velocity and surfactant concentration, following the approach of Erneux and Davis. Sharma et al.[42] carried out a weakly nonlinear analysis of thin freestanding liquid films and numerically solved the coupled nonlinear evolution equations. Matar[43] investigated the nonlinear evolution of thin freestanding films in the presence of soluble surfactants in two limits: slow and rapid bulk diffusion. The results showed that rupture is promoted through an increase in magnitude of van der Waals forces and surfactant solubility and is retarded via an increase in Marangoni forces and surface viscosity.

The above studies are largely confined to thin Newtonian freestanding films. Most of the applications of thin films involve polymeric liquids which are viscoelastic in nature. Nevertheless, there have been a few studies that addressed the effect of elasticity in both supported and freestanding

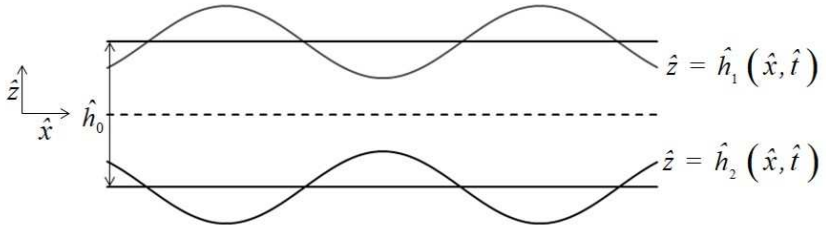

FIG. 1. Schematic representation of an undulating thin freestanding film in squeezing mode. The dotted line at the center of the film represents the origin of the considered Cartesian coordinate system. The upper and the lower deforming interfaces of the freestanding film are located at $\hat{z} = \hat{h}_1(\hat{x},\hat{t})$ and $\hat{z} = \hat{h}_2(\hat{x},\hat{t})$, respectively. The solid straight lines represent the mean positions of the deforming interfaces at $\hat{z} = \pm\hat{h}_0/2$.

films. Zhang et al.[45] used the Ostwald constitutive relation to model the precorneal mucus coating while studying its rupture mechanism. Rauscher et al.[46] derived a thin film equation based on linear Jeffreys model and showed that rim profile always has an oscillatory behavior during dewetting. Tomar et al.[31] studied the instability and dynamics of thin Jeffreys viscoelastic supported film using linear stability and nonlinear simulations and showed that the liquid viscoelasticity does not alter the length scale of instability but significantly enhances the growth rate of disturbances. Sarkar and Sharma[47] formulated a unified theory of field-induced instabilities in thin viscoelastic films. They carried out both linear stability analysis of a linear viscoelastic solid thin film subjected to an arbitrary force field and nonlinear simulations of purely elastic films. Patra et al.[33] extended the linear theory of Sarkar and Sharma and studied the nonlinear stability and dewetting of zero-frequency viscoelastic solid thin film on uniform and patterned surfaces. Barra et al.[48] investigated the effects of viscoelasticity and substrate slippage on the dynamics of thin Jeffreys viscoelastic films. Their results show that viscoelastic parameters and slip length do not alter the length scale of the instability, but affect the time scale. Bazzi and Carvalho[44] studied the effect of viscoelastic forces on the rupture process of a liquid sheet using numerical simulations and showed that the rheology of the liquid does not affect the stability criterion, but has a strong effect on the growth rate of the disturbance and the consequent rupture time.

In the present study, we investigate the instability of thin freestanding films under the influence of attractive van der Waals forces for three different rheological models viz., viscous films, zero-frequency viscoelastic solid films, and Jeffreys viscoelastic liquid films. The goal of the present effort is to elucidate and distinguish the role of rheology on the instability in such systems. The rest of this article is organized as follows. In Sec. II, we present the dimensional governing equations and the boundary conditions for the rheological models considered. Dimensionless scales are given in Sec. III. In Sec. IV, the resulting dimensionless governing equations and boundary conditions are linearized to obtain the dispersion relations for each rheological model. The linear stability results are discussed in Sec. V and conclusions are given in Sec. VI.

II. PROBLEM FORMULATION

Figure 1 presents the schematic of a thin viscoelastic freestanding film of thickness $\hat{h}_0$ which is bounded by a passive gas on either side. In the present formulation, a two-dimensional Cartesian coordinate system is employed to model the thin freestanding film. Here, $\hat{x}$ and $\hat{z}$ represent the abscissa and ordinate and the variable $\hat{t}$ represents time. A hat over the variable indicates that it

is a dimensional quantity. In a thin freestanding film, the perturbed upper and lower interfaces are located at $\hat{z} = \hat{h}_1(\hat{x}, \hat{t})$ and $\hat{z} = \hat{h}_2(\hat{x}, \hat{t})$ respectively which undulate around their mean positions at $\hat{z} = \pm\hat{h}_0/2$. The local film thickness at any instant of time is denoted by $\hat{h}_f(\hat{x}, \hat{t})$ and can be obtained from the difference in positions of upper and lower interfaces $\hat{h}_f(\hat{x}, \hat{t}) = \hat{h}_1(\hat{x}, \hat{t}) - \hat{h}_2(\hat{x}, \hat{t})$. Even in the absence of any external body forces, thin films are rendered unstable due to the amplification of spontaneous disturbances by attractive van der Waals interactions[36]. The disjoining pressure, which is the excess pressure in the thin film compared to the bulk phase, at either of the interfaces, is given as $\hat{\pi}_f = -\hat{A}/(6\pi\hat{h}_f^3)$, where $\hat{A}$ is the Hamaker constant. A negative disjoining pressure (positive Hamaker constant) causes the spontaneous thinning of the film leading to film rupture. The continuum description of thin film flow can be accomplished by solving the governing momentum balance equation augmented by a body force due to van der Waals interactions, which have to be solved along with the equation of continuity, kinematic condition, tangential and normal stress boundary conditions at both the interfaces. The film is assumed to be thin enough such that the intermolecular van der Waals forces become dominant over the gravitational forces and thick enough that a continuum theory is applicable. The film is also considered to be incompressible and isothermal. Unlike in the study of instability of thin supported films where the inertial terms are usually neglected, they need to be retained in the governing equations of thin freestanding films[40,42]. This is necessary for capturing the dominant length scale of instability. Instability of thin freestanding films with three different rheological descriptions, viz., purely viscous, zero-frequency viscoelastic solid and Jeffreys viscoelastic liquid, is investigated in the present work. Separate formulations of the governing equations and boundary conditions for each rheology are presented in this section. Vector quantities are denoted by bold variables whereas tensor quantities are denoted by bold face Greek alphabets. The variables with an over-dot represent the partial time derivative. Subscripts *i* = 1 and 2 denote the upper and lower interfaces respectively. In the governing equations $\frac{D}{Dt}$ indicates the substantial derivate and $\hat{\nabla}\{\partial_{\hat{x}}, \partial_{\hat{z}}\}$ is the gradient operator.

A. Viscous freestanding film

The equations of motion which describe the dynamics of a thin freestanding viscous film along with the corresponding constitutive relation are:

$$\hat{\nabla} \cdot \hat{\mathbf{v}} = 0, \tag{1}$$

$$-\hat{\nabla}\hat{p} + \hat{\nabla} \cdot \hat{\boldsymbol{\sigma}}_{\boldsymbol{v}} = \hat{\rho}\frac{D\hat{\mathbf{v}}}{D\hat{t}}, \tag{2}$$

$$\hat{\boldsymbol{\sigma}}_v = \hat{\mu}\left(\hat{\nabla}\hat{\mathbf{v}} + \hat{\nabla}\hat{\mathbf{v}}^T\right). \tag{3}$$

The following tangential, normal stress balances and the kinematic conditions are enforced as boundary conditions at the free interfaces located at $\hat{z} = \hat{h}_i(\hat{x}, \hat{t})$:

$$\hat{\mathbf{t}}_i \cdot \hat{\boldsymbol{\sigma}}_{\boldsymbol{v}} \cdot \hat{\mathbf{n}}_i = 0, \tag{4}$$

$$-\hat{p}_f + \hat{\mathbf{n}}_i \cdot \hat{\boldsymbol{\sigma}}_{\boldsymbol{v}} \cdot \hat{\mathbf{n}}_i = \pm\hat{\gamma}\hat{\kappa}_i, \tag{5}$$

$$\dot{\hat{h}}_i + \hat{\mathbf{v}} \cdot \hat{\nabla}\hat{h}_i = \hat{v}_z. \tag{6}$$

Here, the symbols $\hat{\mathbf{v}}\{\hat{v}_x, \hat{v}_z\}$, $\hat{p}$, $\hat{\boldsymbol{\sigma}}_{\boldsymbol{v}}$, $\hat{\rho}$, $\hat{\mu}$, and $\hat{\gamma}$ represent the velocity vector, total pressure, stress tensor, denisty, viscosity, and surface tension respectively. The total pressure ($\hat{p} = \hat{p}_f - \hat{\pi}_f$) in the thin film is the sum of fluid pressure ($\hat{p}_f$) and negative disjoining pressure (–$\hat{\pi}_f$). The surface tension is assumed to be constant and thus Marangoni stresses are neglected leading to a vanishing

shear stress at the interface. The symbols $\hat{\mathbf{n}}_i$ and $\hat{\mathbf{t}}_i$ are the unit outward normal and tangential vectors at the interfaces which are defined as $\hat{\mathbf{n}}_i = \{\hat{\nabla}(\hat{z} - \hat{h}_i)/|\hat{\nabla}(\hat{z} - \hat{h}_i)|\}$ and $\hat{\mathbf{n}}_i \cdot \hat{\mathbf{t}}_i = 0$. The curvature of freestanding surfaces is given by $\hat{\kappa}_i = \hat{\nabla} \cdot \hat{\mathbf{n}}_i$.

B. Zero-frequency viscoelastic solid freestanding film

The constitutive relation of a zero-frequency viscoelastic solid (see Eq. (9) below) represents a linear combination of Hookean elastic spring and viscous dashpot connected in parallel. The equations of motion which describe the dynamics of a thin freestanding zero-frequency viscoelastic solid film along with the corresponding constitutive relation are:

$$\hat{\nabla} \cdot \hat{\mathbf{u}} = 0, \tag{7}$$

$$-\hat{\nabla}\hat{p} + \hat{\nabla} \cdot \hat{\boldsymbol{\sigma}}_{\boldsymbol{s}} = \hat{\rho}\frac{D\hat{\hat{\mathbf{u}}}}{D\hat{t}}, \tag{8}$$

$$\hat{\boldsymbol{\sigma}}_s = \hat{G}\left(\hat{\nabla}\hat{\mathbf{u}} + \hat{\nabla}\hat{\mathbf{u}}^T\right) + \hat{\mu}\left(\hat{\nabla}\hat{\dot{\mathbf{u}}} + \hat{\nabla}\hat{\dot{\mathbf{u}}}^T\right). \tag{9}$$

The following tangential, normal stress balances and the kinematic conditions are enforced as boundary conditions at the interfaces, of a freestanding solid film, located at $\hat{z} = \hat{h}_i(\hat{x}, \hat{t})$:

$$\hat{\mathbf{t}}_i \cdot \hat{\boldsymbol{\sigma}}_{\boldsymbol{s}} \cdot \hat{\mathbf{n}}_i = 0, \tag{10}$$

$$-\hat{p}_f + \hat{\mathbf{n}}_i \cdot \hat{\boldsymbol{\sigma}}_{\boldsymbol{s}} \cdot \hat{\mathbf{n}}_i = \pm\hat{\gamma}\hat{\kappa}_i, \tag{11}$$

$$\hat{\dot{h}}_i + \hat{\mathbf{u}} \cdot \hat{\nabla}\hat{h}_i = \hat{w}. \tag{12}$$

Here, the symbols $\hat{\mathbf{u}}\{\hat{u}, \hat{w}\}$, $\hat{\boldsymbol{\sigma}}_{\boldsymbol{s}}$ and $\hat{G}$ represent the displacement vector, stress tensor for a zero-frequency viscoelastic solid and shear modulus respectively.

C. Jeffreys viscoelastic liquid freestanding film

In addition to the above models, Jeffreys linear viscoelastic model is used to describe a thin freestanding viscoelastic liquid film. Jeffreys model uses a single relaxation time constant similar to Maxwell model. Jeffreys model has an additional term with retardation time constant in its constitutive relation. Thus, the Jeffreys model reduces to the Maxwell model in the zero retardation time constant limit. The relaxation time constant used in these models is interpreted as the largest relaxation time constant in the original spectrum of relaxation times exhibited by a real polymeric liquid[31]. Both Maxwell and Jeffreys models use a simple time derivative for the stress tensor in the constitutive relation and when the same is replaced by the corotational derivative, these models are referred to as upper-convected Maxwell model and Oldroyd-B model respectively[49].
The equations of motion which describe the dynamics of a thin Jeffreys viscoelastic liquid freestanding film along with the corresponding constitutive relation are:

$$\hat{\nabla} \cdot \hat{\mathbf{v}} = 0, \tag{13}$$

$$-\hat{\nabla}\hat{p} + \hat{\nabla} \cdot \hat{\boldsymbol{\sigma}}_{\boldsymbol{l}} = \hat{\rho}\frac{D\hat{\mathbf{v}}}{D\hat{t}}, \tag{14}$$

$$\hat{\boldsymbol{\sigma}}_l + \hat{\lambda}_1\hat{\boldsymbol{\sigma}}_l = \hat{\mu}\left((\hat{\nabla}\hat{\mathbf{v}} + \hat{\nabla}\hat{\mathbf{v}}^T) + \hat{\lambda}_2\partial_{\hat{t}}(\hat{\nabla}\hat{\mathbf{v}} + \hat{\nabla}\hat{\mathbf{v}}^T)\right). \tag{15}$$

Here, the symbols $\hat{\boldsymbol{\sigma}}_{\boldsymbol{l}}$, $\hat{\lambda}_1$ and $\hat{\lambda}_2$ represent stress tensor for a Jeffreys viscoelastic liquid, relaxation time and retardation time respectively. In the above constitutive relation, the total viscosity ($\hat{\mu} = \hat{\mu}_p + \hat{\mu}_s$), is the sum of viscosities due to polymer and solvent contributions. A parameter, viscosity ratio μ_r, is defined here as the fraction of solvent contribution to the total viscosity. The retardation and relaxation time constants are related in the following manner

$$\hat{\lambda}_2 = \hat{\lambda}_1 \mu_r. \tag{16}$$

The boundary conditions at the free interfaces ($\hat{z} = \hat{h}_i(\hat{x}, \hat{t})$) of a Jeffreys viscoelastic freestanding film are same as that of a viscous freestanding film (Eqs. (4) - (6)), except for the change in stress tensor.

D. Excess pressure at the interfaces

In the present problem formulation, the symmetry condition is not imposed and both the interfaces of the film undulate around their respective mean positions located at $\hat{z} = \pm\hat{h}_0/2$. The disjoining pressure ($\hat{\pi}_f$), is a function of local film thickness ($\hat{h}_f = \hat{h}_1 - \hat{h}_2$) at any instant of time,

$$\hat{\pi}_f(\hat{h}_1,\, \hat{h}_2) = \frac{-\hat{A}}{6\pi(\hat{h}_1 - \hat{h}_2)^3}\,. \tag{17}$$

The functions $\hat{\delta}_1(\hat{x}, \hat{t})$ and $\hat{\delta}_2(\hat{x}, \hat{t})$ are defined as the infinitesimal perturbations at the upper and lower interfaces, respectively. Now the disjoining pressure is expanded in multivariate Taylor series around the base state and the terms up to first order are retained to obtain,

$$\hat{\pi}_f\left(\frac{\hat{h}_0}{2} + \hat{\delta}_1,\, -\frac{\hat{h}_0}{2} + \hat{\delta}_2\right) = \hat{\pi}_f\left(\frac{\hat{h}_0}{2}, -\frac{\hat{h}_0}{2}\right) + \left[\left(\frac{\partial\hat{\pi}_f}{\partial h_1}\right)\hat{\delta}_1 + \left(\frac{\partial\hat{\pi}_f}{\partial h_2}\right)\hat{\delta}_2\right]. \tag{18}$$

The first term on the right-hand side in Eq. (18) represents the base state term. The second term on the right-hand side in this equation is further simplified by expressing it in terms of interaction stiffness ($\hat{Y}$) which is defined as,

$$\hat{Y} = -\frac{\partial\hat{\pi}_f}{\partial\hat{h}_f}\Big|_{\hat{h}_f=\hat{h}_0} = -\frac{\hat{A}}{2\pi\hat{h}_0^4}. \tag{19}$$

Using Eq. (19) and using the chain rule of partial differentiation, the disjoining pressure given by Eq. (18) simplifies as,

$$\hat{\pi}_f = \hat{Y}(\hat{\delta}_2 - \hat{\delta}_1). \tag{20}$$

III. DIMENSIONLESS FORMS

We assume that the thin film has a kinematic viscosity $\hat{\nu}$ and a constant density $\hat{\rho}$. The governing equations and the boundary conditions presented in Sec. II are made dimensionless using the following scales: length (or displacement) $\sim \hat{h}_0$, time $\sim \hat{h}_0^2/\hat{\nu}$, velocity $\sim \hat{\nu}/\hat{h}_0$, surface tension $\sim \hat{\rho}\hat{\nu}^2/\hat{h}_0$, shear modulus and pressure $\sim \hat{\rho}\hat{\nu}^2/\hat{h}_0^2$. The nondimensional variables / parameters employing the above scales are: $(h_1, h_2, \delta_1, \delta_2) = (\hat{h}_1, \hat{h}_2, \hat{\delta}_1, \hat{\delta}_2)/\hat{h}_0$; $(x, z) = (\hat{x}, \hat{z})/\hat{h}_0$; $\mathbf{u}\{u, w\} = \hat{\mathbf{u}}\{\hat{u}, \hat{w}\}/\hat{h}_0$; $\dot{\mathbf{u}}\{\dot{u}, \dot{w}\} = \hat{\dot{\mathbf{u}}}\{\hat{\dot{u}}, \hat{\dot{w}}\}\,\hat{h}_0/\hat{\nu}$; $\mathbf{v}\,\{v_x, v_z\} = \hat{\mathbf{v}}\,\{\hat{v}_x, \hat{v}_z\}\,\hat{h}_0/\hat{\nu}$; $(t, \lambda_1, \lambda_2) = \left(\hat{t}, \hat{\lambda}_1, \hat{\lambda}_2\right)\hat{\nu}/\hat{h}_0^2$; $\gamma = \hat{\gamma}\hat{h}_0/\hat{\rho}\hat{\nu}^2$; $G = \hat{G}\hat{h}_0^2/\hat{\rho}\hat{\nu}^2$; $Y = \hat{Y}\hat{h}_0^3/\hat{\rho}\hat{\nu}^2$; $(p, p_f, \phi) = (\hat{p}, \hat{p}_f, \hat{\phi})\hat{h}_0^2/\hat{\rho}\hat{\nu}^2$; $(\boldsymbol{\sigma}_v, \boldsymbol{\sigma}_s, \boldsymbol{\sigma}_l) = (\hat{\boldsymbol{\sigma}}_v, \hat{\boldsymbol{\sigma}}_s, \hat{\boldsymbol{\sigma}}_l)\hat{h}_0^2/\hat{\rho}\hat{\nu}^2$; and $A = \hat{A}/\left(6\pi\hat{\rho}\hat{\nu}^2\hat{h}_0\right)$.

IV. LINEAR STABILITY ANALYSIS

In this section, we carry out the general linear stability of the thin freestanding film and derive the dispersion relation for the three rheological models considered in the present study. In order to carry out the linear stability analysis of a thin freestanding film subjected to infinitesimal arbitrary disturbances, the governing equations and the corresponding boundary conditions are linearized using the normal linear modes, $\mathbf{v} = \tilde{\mathbf{v}}\, e^{\omega t+ikx}$, $\mathbf{u} = \tilde{\mathbf{u}}\, e^{\omega t+ikx}$, $\sigma_{*ij} = \tilde{\sigma}_{*ij}\, e^{\omega t+ikx}$ (* = *v* / *s* / *l*), $p = \tilde{p}\, e^{\omega t+ikx}$, and $h_i = \pm\frac{1}{2} + \tilde{\delta}_i\, e^{\omega t+ikx}$ where ω and *k* denote the linear growth coefficient and wave number of the disturbance respectively. The variables $\tilde{\mathbf{v}}$, $\tilde{\mathbf{u}}$, $\tilde{\sigma}_{*ij}$, and $\tilde{p}$, are the amplitudes of perturbation of the respective variables which are exclusive functions of the ordinate. The symbol $\tilde{\delta}_i$ represents the amplitude of infinitesimal perturbation in height at the upper ($i = 1$) and lower ($i = 2$) interfaces.

A. Viscous freestanding film

The governing equations of thin freestanding viscous film, Eqs. (1) - (3) are made dimensionless using the nondimensional scales given in Sec. III and linearized to obtain the following expressions:

$$-ik\,\tilde{p} + \left(-k^2\tilde{v}_x + \frac{\partial^2\tilde{v}_x}{\partial z^2}\right) = \tilde{v}_x\omega\,, \tag{21}$$

$$-\frac{\partial\tilde{p}}{\partial z} + \left(-k^2\tilde{v}_z + \frac{\partial^2\tilde{v}_z}{\partial z^2}\right) = \tilde{v}_z\omega\,, \tag{22}$$

$$ik\tilde{v}_x + \frac{\partial\tilde{v}_z}{\partial z} = 0\,. \tag{23}$$

Eliminating $\tilde{p}$ from the Eqs. (21) and (22) and then replacing $\tilde{v}_x$ in terms of $\tilde{v}_z$ from Eq. (23), we obtain the following biharmonic equation for the thin freestanding viscous film which is given as

$$\frac{d^4\tilde{v}_z}{dz^4} - \left(2k^2+\omega\right)\frac{d^2\tilde{v}_z}{dz^2} + k^2\left(k^2+\omega\right)\tilde{v}_z = 0. \tag{24}$$

The general solution of Eq. (24) is given as

$$\tilde{v}_z = B_1 e^{z\sqrt{k^2+\omega}} + B_2 e^{-z\sqrt{k^2+\omega}} + B_3 e^{kz} + B_4 e^{-kz}. \tag{25}$$

Here, the coefficients B_i (i =1 to 4) are constants. These four constants can be obtained from the four boundary conditions, i.e., tangential and normal stress balances at both the free interfaces. The linearized tangential, normal stress conditions and kinematic conditions at $z = h_i(x,t)$ are,

$$\frac{\partial\tilde{v}_x}{\partial z} + ik\,\tilde{v}_z = 0, \tag{26}$$

$$\tilde{p}_f - 2\frac{\partial\tilde{v}_z}{\partial z} \pm \gamma k^2\tilde{\delta}_i = 0, \tag{27}$$

$$\tilde{\delta}_i = \left.\frac{\tilde{v}_z}{\omega}\right|_{z=\pm 0.5}. \tag{28}$$

By definition, the total pressure (p), is a sum of isotropic film pressure (p_f) and negative disjoining pressure ($-\pi_f$). Now using Eq. (20) in the linearized nondimensional form, the $\tilde{p}_f$ in Eq. (27) can be expressed as

$$\tilde{p}_f = \tilde{p} + Y(\tilde{\delta}_2 - \tilde{\delta}_1). \tag{29}$$

We have the expression for $\tilde{v}_z$, in the form of solution to the biharmonic equation, which is given by Eq. (25). The expression for $\tilde{p}$ can be obtained from Eq.(21). Substituting the expressions for $\tilde{v}_z$, $\tilde{v}_x$, and $\tilde{p}$ in the linearized boundary conditions results in a set of four homogeneous algebraic equations involving four unknown constants B_i (i =1 to 4). Equating the determinant of the coefficient matrix of these set of four linear homogeneous algebraic equations to zero, the dispersion relation ($f(\omega, k)$) for the thin freestanding viscous film is obtained. From the dispersion relation, it is evident that linear growth coefficient (ω) cannot be expressed as an explicit function of the wavenumber k. The solution of the dispersion relation is obtained by numerically solving it for each k using Mathematica. We have used the Newton-Raphson iteration scheme with an initial guess to solve the resulting transcendental equation for ω. The numerical solution of the dispersion relation $f(\omega, k)$ is used to obtain the ω-k dispersion curves, from which the maximum growth rate, ω_m and the corresponding dominant wavelength, λ_m are obtained.

B. Zero-frequency viscoelastic solid freestanding film

The governing equations of a thin freestanidng zero-frequency viscoelastic solid film, Eqs. (7) - (9) are made dimensionless using the nondimensional scales given Section III and are linearized using the normal linear modes to obtain the following equations:

$$-ik\,\tilde{p} + (G+\omega)\left(-k^2\tilde{u} + \frac{\partial^2\tilde{u}}{\partial z^2}\right) - \tilde{u}\omega^2 = 0\,, \tag{30}$$

$$-\frac{\partial\tilde{p}}{\partial z} + (G+\omega)\left(-k^2\tilde{w} + \frac{\partial^2\tilde{w}}{\partial z^2}\right) - \tilde{w}\omega^2 = 0\,, \tag{31}$$

$$ik\,\tilde{u} + \frac{\partial\tilde{w}}{\partial z} = 0\,. \tag{32}$$

The biharmonic equation for a thin freestanding zero-frequency viscoelastic solid film obtained from Eqs. (30) - (32) is,

$$\frac{d^4\tilde{w}}{dz^4} - \left(2k^2 + \frac{\omega^2}{(G+\omega)}\right)\frac{d^2\tilde{w}}{dz^2} + k^2\left(k^2 + \frac{\omega^2}{(G+\omega)}\right)\tilde{w} = 0. \tag{33}$$

For the sake of convenience, let us define a parameter r as,

$$r = \frac{\omega}{\sqrt{(G+\omega)}}. \tag{34}$$

The general solution of Eq. (33) is given as,

$$\tilde{w} = C_1 e^{z\sqrt{k^2+r^2}} + C_2 e^{-z\sqrt{k^2+r^2}} + C_3 e^{kz} + C_4 e^{-kz}. \tag{35}$$

The constants C_i (i =1 to 4) are obtained from the four boundary conditions, i.e., tangential and normal stress balances at both the free interfaces. The linearized tangential, normal stress conditions and kinematic conditions at $z = h_i(x,t)$ are,

$$(G+\omega)\,\left(\frac{\partial\tilde{u}}{\partial z} + ik\,\tilde{w}\right) = 0, \tag{36}$$

$$\tilde{p}_f - 2\,(G+\omega)\frac{\partial\tilde{w}}{\partial z} \pm \gamma k^2\tilde{\delta}_i = 0, \tag{37}$$

$$\tilde{\delta}_i = \tilde{w}|_{z=\pm 0.5}\,. \tag{38}$$

C. Jeffreys viscoelastic liquid freestanding film

The constitutive relation for a thin freestanding Jeffreys viscoelastic liquid film Eq. (15), is made dimensionless using the nondimensional scales given in Sec. III and is linearized using the normal linear modes to obtain the following linearized components of the stress tensor $\tilde{\boldsymbol{\sigma}}_l$:

$$\tilde{\sigma}_{l\,xx} = 2\,\frac{[1+\lambda_1\mu_r\omega]}{[1+\lambda_1\omega]}\;(ik)\;\tilde{v}_x\,, \tag{39}$$

$$\tilde{\sigma}_{l\,xz} = \tilde{\sigma}_{l\,zx} = \;\frac{[1+\lambda_1\mu_r\omega]}{[1+\lambda_1\omega]}\;\left(\frac{\partial\tilde{v}_x}{\partial z} + ik\,\tilde{v}_z\right), \tag{40}$$

$$\tilde{\sigma}_{l\,zz} = 2\,\frac{[1+\lambda_1\mu_r\omega]}{[1+\lambda_1\omega]}\;\frac{\partial\tilde{v}_z}{\partial z}\,. \tag{41}$$

The linearized forms of x- and z- momentum equations and continuity equation, which describe the dynamics of thin freestanding Jeffreys viscoelastic liquid film are,

$$-k^2\tilde{p} + \frac{[1+\lambda_1\mu_r\omega]}{[1+\lambda_1\omega]}\left(\frac{\partial^3\tilde{v}_z}{\partial z^3} - k^2\frac{\partial\tilde{v}_z}{\partial z}\right) = \omega\frac{\partial\tilde{v}_z}{\partial z}, \tag{42}$$

$$-\frac{\partial\tilde{p}}{\partial z} + \frac{[1+\lambda_1\mu_r\omega]}{[1+\lambda_1\omega]}\left(\frac{\partial^2\tilde{v}_z}{\partial z^2} - k^2\tilde{v}_z\right) = \omega\;\tilde{v}_z, \tag{43}$$

$$ik\,\tilde{v}_x + \frac{\partial\tilde{v}_z}{\partial z} = 0\,. \tag{44}$$

Eliminating $\tilde{p}$ from the Eqs. (42) and (43), we obtain the following biharmonic equation for the thin Jeffreys viscoelastic solid freestanding film:

$$\frac{d^4\tilde{v}_z}{dz^4} - \left[2k^2 + \frac{\omega\,(1+\lambda_1\omega)}{(1+\lambda_1\mu_r\omega)}\right]\frac{d^2\tilde{v}_z}{dz^2} + k^2\left[k^2 + \frac{\omega\,(1+\lambda_1\omega)}{(1+\lambda_1\mu_r\omega)}\right]\tilde{v}_z = 0. \tag{45}$$

For the sake of convenience, let us define two parameters α and f as,

$$\alpha = \frac{(1+\lambda_1\mu_r\omega)}{(1+\lambda_1\omega)} \text{ and } f = \sqrt{\frac{\omega}{\alpha}}. \tag{46}$$

The general solution of the biharmonic equation, Eq. (45) is given as,

$$\tilde{v}_z = D_1 e^{z\sqrt{k^2+f^2}} + D_2 e^{-z\sqrt{k^2+f^2}} + D_3 e^{kz} + D_4 e^{-kz}. \tag{47}$$

The constants D_i ($i = 1$ to 4) are obtained from the boudnary conditions, i.e., tangential and normal stress balances at both the free interfaces. The linearized tangential, normal stress conditions and kinematic conditions at $z = h_i(x,t)$ are,

$$\frac{\partial\tilde{v}_x}{\partial z} + ik\,\tilde{v}_z\; = 0, \tag{48}$$

$$\tilde{p}_f - 2\alpha\frac{\partial\tilde{v}_z}{\partial z} \pm \gamma k^2\tilde{\delta}_i = 0, \tag{49}$$

$$\tilde{\delta}_i = \left.\frac{\tilde{v}_z}{\omega}\right|_{z=\pm 0.5}. \tag{50}$$

D. Relative deformations at the interfaces of the freestanding film

The two free interfaces of a thin freestanding film can deform through either in phase bending mode (stretching mode) or out phase squeezing mode (symmetric mode). However, the freestanding film system considered here is a symmetrical system[21], and we can observe from Eq. (20), that the excess pressure term which engenders the instability, vanishes when the amplitudes of disturbances at the interfaces are equal. Thus this equation hints that a bending mode of deformation with equal amplitudes at the interfaces does not occur here. The mode of deformation of the freestanding film is not imposed here a priori in our analysis but is evaluated from the sign and magnitude of the amplitude ratio. The procedure to obtain amplitude ratio is similar to the one followed for bilayers[50] and is illustrated here for a thin freestanding viscous film.

The amplitudes of perturbation in height at the two free interfaces are $\tilde{\delta}_1$ and $\tilde{\delta}_2$ for the upper and lower interfaces, respectively. The amplitude ratio ($\delta_r = \tilde{\delta}_1/\tilde{\delta}_2$), is evlauated using the linearized boundary conditions, Eqs. (26) - (28).

From the linearized kinematic conditions and tangetial stress balances at both the interfaces, we have the following four linear algebraic equations:

$$\tilde{v}_z\,|_{z=0.5} = \tilde{\delta}_1\omega, \tag{51a}$$

$$\tilde{v}_z\,|_{z=-0.5} = \tilde{\delta}_2\omega. \tag{51b}$$

$$\frac{\partial \tilde{v}_x}{\partial z}\,|_{z=0.5} + ik\,\tilde{v}_z\,|_{z=0.5} = 0, \tag{52a}$$

$$\frac{\partial \tilde{v}_x}{\partial z}\,|_{z=-0.5} + ik\,\tilde{v}_z\,|_{z=-0.5} = 0. \tag{52b}$$

Here, $\tilde{v}_z|_{z=\pm 0.5}$ is known from the solution of the biharmonic equation for thin freestanding viscous film which is given by Eq. (25). Now, the set of four linear equations, Eqs. (51) and (52), are solved to obtain the four unknown constants B_i (i =1−4). Maximum growth rate (ω_m) and the corresponding dominant wave number (k_m) are obtained by finding the global maximum of the solution of the dispersion relation. The constants, B_i evaluated at dominant mode now become $f(\tilde{\delta}_1, \tilde{\delta}_2)$. Amplitude ratio is finally obtained from the normal stress balance at either interface.

The sign of δ_r evaluated at dominant growth rate gives us the information regarding whether the fastest mode of instability is bending or squeezing in nature whereas the magnitude of δ_r tells us the relative amplitudes of disturbances at the interfaces. A squeezing mode of deformation results when $\delta_r < 0$ and a bending mode of deformation occurs when $\delta_r > 0$. Equal deformations happen at the interfaces when the magnitude of amplitude ratio, $|\delta_r| = 1$, and any deviation from unity indicates unequal deformations at the interfaces.

V. RESULTS AND DISCUSSION

In this section, linear stability analysis (LSA) results of a thin freestanding film under the influence of attractive van der Waals interactions are presented for the three rheologies viz., viscous, zero-frequency viscoelastic solid and Jeffreys viscoelastic liquid. Thin viscous films are unconditionally unstable unlike viscoelastic solid films which are unstable only when the strength of the destabilizing forces exceeds the strength of stabilizing elastic and surface tension[47]. Unlike solids, wherein elasticity tends to retard the growth rate and governs the onset of instability, elasticity enhances the growth rate in viscoelastic liquids; further there is no threshold for the onset of instability. However, in the case of supported viscoelastic films, rheological details do not alter the

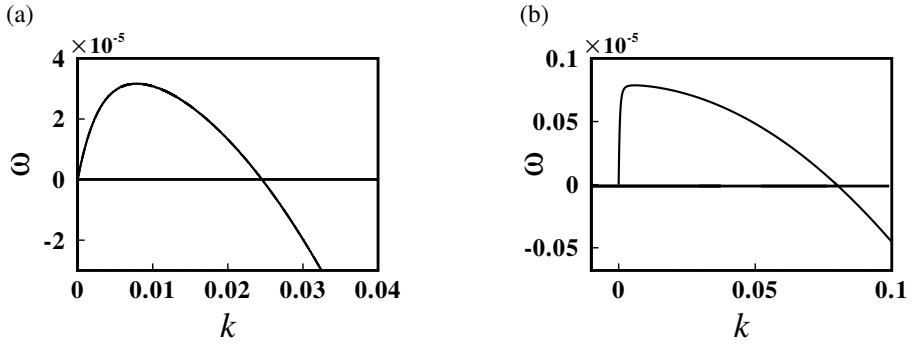

FIG. 2. GLSA of thin freestanding viscous films. Plot (a) shows the ω vs k curve of a 10 nm thin freestanding viscous film, obtained through GLSA for the same set of parameters used by Sharma et al.[42] in their longwave analysis. The parameters used are γ = 0.528 and $A = 5.3 \times 10^{-5}$. Plot (b) shows the ω vs k curve of a 5 nm thin freestanding viscous film for another set of the parameters. The parameters used are γ = 10^{-3} and $A = 1.06 \times 10^{-6}$.

length scale of the instability which is governed by thermodynamic factors like surface tension and destabilizing forces[31,33].

Thin freestanding viscous films[38,41,42] have been studied in detail in the earlier studies using the long-wave linear stability analysis and nonlinear simulations. For freestanding viscous and viscoelastic solid films, GLSA results are briefly presented. Here the major focus is devoted to the study of a thin freestanding Jeffreys viscoelastic liquid film, wherein the effects of Weissenberg number, viscosity ratio and inertia on its instability are investigated and compared with the results of a thin supported Jeffreys viscoelastic liquid[31]. The Hamaker constant ($\hat{A}$) is taken to be 10^{-20} J in all the plots.

A. Viscous freestanding film

The LSA results of a thin freestanding viscous film are shown in Figure 2. Figures 2(a) and 2(b) show the variation of growth rate (ω) with the wavenumber (k) for two different parameter sets. The dominant mode of instability for a thin freestanding film can be captured through retention of the inertial terms in Eqs. (21) and (22). If we neglect the inertial terms in a freestanding film, it is observed that maximum growth rate occurs at $k = 0$. Figure 2(a) shows the GLSA result of a thin freestanding viscous film, for the same set of parameters used by Sharma et al.[42] in their long-wave linear stability analysis of thin freestanding viscous films. It can be seen that the ω vs k curve obtained through GLSA exactly matches with the long-wave linear stability result. Figure 2(b) shows the ω vs k curve obtained using GLSA for another set of parameter values. In comparison with the ω vs k curve in Figure 2(a), the domain of instability is increased in Figure 2(b) due to lower surface tension forces $\left(\text{cutoff wavenumber, } k_c \sim \gamma^{-1/2}\right)$. However, the dominant growth rate is decreased in this case due to increase in viscous forces. The dominant wavenumber in Figure 2(b) shifts towards the longer wavelengths in comparison with Figure 2(a).

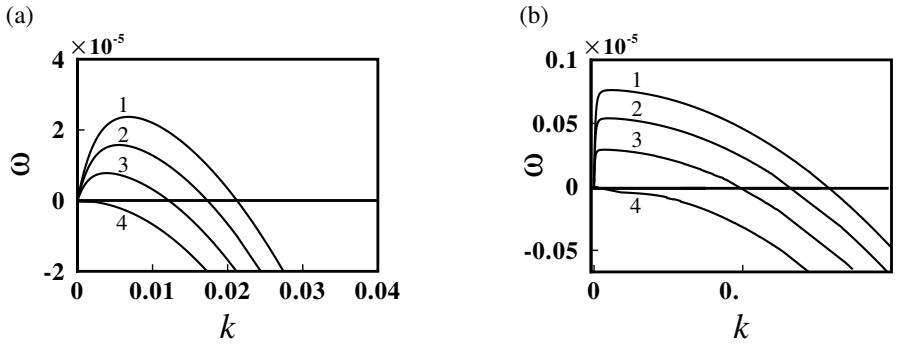

FIG. 3. GLSA of thin freestanding viscoelastic solid films. Plot (a) shows ω vs k curves of a 10 nm thin freestanding viscoelastic solid film at different values of G. Curves 1–4 represent $G = 10^{-5}$, 2×10^{-5}, 3×10^{-5} and 3.98×10^{-5} respectively. Plot (b) shows ω vs k curves of a 5 nm thin freestanding viscoelastic solid film at different values of G. Curves 1–4 represent $G = 2.5 \times 10^{-8}$, 2.5×10^{-7}, 5×10^{-7}, and 8×10^{-7} respectively. Parameters γ and A in plots (a) and (b) are the same as used in Figure 2(a) and Figure 2(b).

B. Zero-frequency viscoelastic solid freestanding film

Unlike thin viscous films which are unconditionally unstable, the instability in thin viscoelastic solid films is engendered when the interaction stiffness of the destabilizing forces overcomes the sum of stabilizing elastic forces and surface tension forces. Thus, there exists a critical shear modulus below which the film is unstable for a given set of parameters. Figure 3 shows the GLSA results of a thin freestanding viscoelastic solid film for two different sets of parameters. It can be seen from Figures 3(a) and 3(b) that elasticity in a thin freestanding viscoelastic solid film has a stabilizing effect (curves 1-3) and governs the onset of instability (curve 4). We can also see from Figure 3(a) that the dominant length scale increases and growth rate decreases with increase in shear modulus which indicates weakening of instability. The elasticity of solid in a thin freestanding film affects both the length scale and time scale of instability and also governs the onset of the same. Thin supported viscoelastic solid films[33] also exhibit the instability only below a critical shear modulus and the instability zone for these films is confined between two neutral wavenumbers. Thus, thin supported viscoelastic solid films exhibit a finite wavenumber instability whereas thin freestanding viscoelastic solid films are unstable even for longer wavelengths below the critical shear modulus. It is noteworthy to mention that the elasticity of solid in thin supported viscoelastic films does not alter the dominant length scale of instability.[33]

C. Jeffreys viscoelastic liquid freestanding film

The GLSA results of a thin freestanding Jeffreys viscoelastic film are compared with those of thin supported Jeffreys viscoelastic film[31] in the zero-inertia limit. In this section, same nondimensional forms for relaxation time and viscosity ratio are followed as used by Tomar et al.[31], but a different nondimensionalization is used for the growth rate and wavenumber. The dimensionless parameters that characterize the Jeffreys viscoelastic liquids are Weissenberg number (W) and the viscosity ratio (μ_r). The Weissenberg number is defined as $W = \hat{\lambda}_1 \hat{A}/6\pi\hat{h}_0^3\hat{\mu}\bar{\gamma}$, where the nondimensional energetic parameter $\bar{\gamma}$ is defined as $\bar{\gamma} = 2\pi\hat{h}_0^2\hat{\gamma}/\hat{A}$. Linear stability results of thin

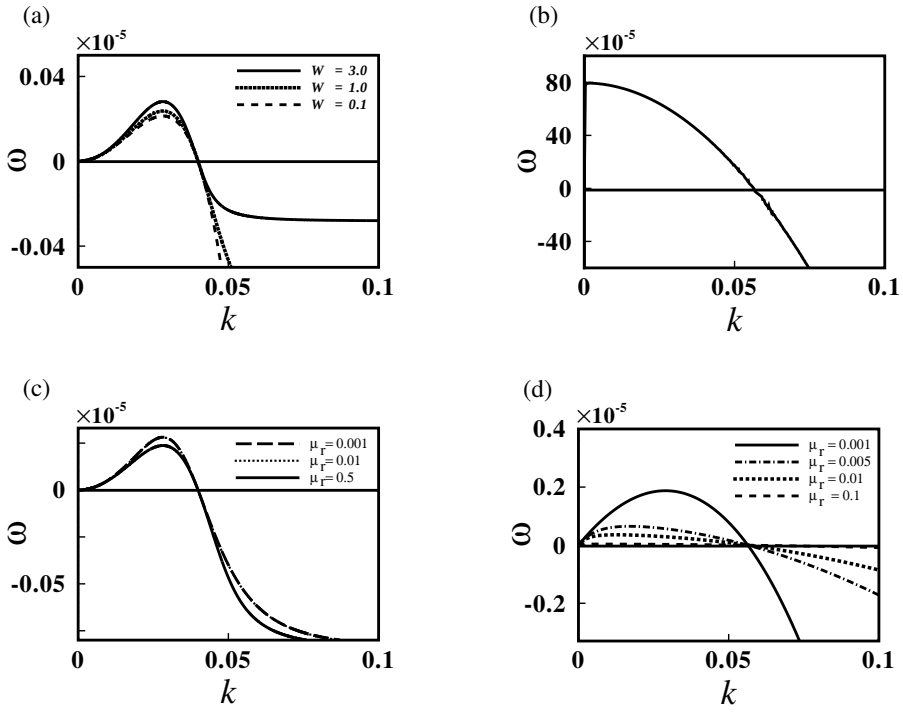

FIG. 4. Comparison of GLSA results of thin freestanding Jeffreys viscoelastic liquid films with thin supported Jeffreys viscoelastic liquid films when $W < 4$. Here, plots (a) and (c) refer to supported viscoelastic liquid films whereas plots (b) and (d) refer to freestanding viscoelastic liquid films. Plots (a) and (b) respectively show the effect of relaxation time on the instability of supported and freestanding viscoelastic liquid films through variation in Weissenberg number (W), at constant viscosity ratio (μ_r = 0.5). Plot (a) shows three ω vs k curves for three different values of W whereas plot (b) shows a single ω vs k curve at the same values of W, indicating that relaxation time does not affect the instability of freestanding viscoelastic liquid films. Plots (c) and (d) respectively show the effect of polymer viscosity on the instability of supported and freestanding viscoelastic liquid films through variation in viscosity ratio (μ_r), at constant Weissenberg number (W = 1). From the ω vs k curves in plots (c) and (d), it can be seen that freestanding viscoelastic liquid films are more sensitive to viscosity ratio than supported viscoelastic liquid films.

freestanding Jeffreys viscoelastic film are presented here with a different nondimensional scaling for the growth rate as $\omega = \hat{\omega}\,(\hat{\mu}\hat{h}_0/\hat{\gamma})$. Typical values of dimensional variables used here are $\hat{h}_0$ = 10 nm, $\hat{\mu}$= 0.1 Pa s and $\hat{\gamma}$ = 0.01 N/m. For supported Jeffreys viscoelastic films as we approach the pure polymer melt regime, it has been found by Tomar et al.[31] that maximum growth rate does not get affected by inclusion or exclusion of inertial terms below a critical value of Weissenberg number ($W = 4$), but beyond this critical value ($W \geqslant 4$) the maximum growth rate predicted using noninertial approximation is unbounded whereas it remains bounded upon inclusion of inertia. In Figure 4, GLSA results of a thin freestanding Jeffreys viscoelastic film are compared with the GLSA results of thin supported Jeffreys viscoelastic film when $W < 4$ (neglecting inertia is valid).

Here, the effect of relaxation time and polymer viscosity on the instability of respective films is studied by varying the parameters W and μ_r independently, while keeping the other parameters constant. Figures 4(a) and 4(b) respectively show the ω vs k curves for supported and freestanding viscoelastic liquid films for different values of Weissenberg number (W) while keeping the viscosity ratio (μ_r) constant. Figure 4(a) shows that the relaxation time enhances the instability for a supported viscoelastic liquid film whereas Figure 4(b) shows that relaxation time does not affect the instability of freestanding viscoelastic liquid film. Similarly, the effect of viscosity ratio (μ_r) on the instability of supported and freestanding viscoelastic liquid films is respectively shown in Figures 4(c) and 4(d) while keeping the Weissenberg number (W) constant. Even though a decrease in (μ_r) enhances the growth rate in both supported and freestanding viscoelastic liquid films, we can see from Figure 4(d) that growth rate of a freestanding viscoelastic liquid film is more sensitive to viscosity ratio. The dominant wave number $\left(k_m = 1/\sqrt{2\bar{\gamma}}\right)$ corresponding to the maximum growth rate of a Jeffreys viscoelastic supported film is unaffected by varying the parameters W and μ_r as can be seen from Figures 4(a) and 4(c). In contrast to supported viscoelastic liquid films, Figure 4(d) shows that with decrease in viscosity ratio, the dominant wavenumber moves towards shorter wavelengths in freestanding viscoelastic liquid films. More than the length scale of instability, the time scale of instability of freestanding viscoelastic liquid films is significantly different from supported viscoelastic liquid films. This can be inferred from the magnitudes of growth rates in Figure 4, which suggest that freestanding viscoelastic liquid films show faster dynamics than supported viscoelastic liquid films. Even though the relaxation time does not affect the instability of freestanding viscoelastic liquid films, increase in polymer contribution to the total viscosity causes the perturbations to grow much faster, especially as we approach pure polymer melt. This finding is consistent with the linear stability results on the instability of thin freestanding viscoelastic liquid sheets[44]. Bazzi and Carvalho,[44] in their work on thin freestanding Maxwell liquid films, found that viscoelastic forces speed up the perturbation growth in the linear regime.

The linear stability results for both supported (without inertia) and freestanding (with inertia) viscoelastic liquid films at larger relaxation times ($W > 4$) are shown in Figure 5. In the absence of inertia, it is known that the response of an elastic solid to an applied force is instantaneous. When the relaxation time in the polymeric liquid is larger than the viscous flow time, the behaviour of a polymeric liquid is similar to an elastic solid. Hence, supported viscoelastic liquid films with larger relaxation times ($W \geqslant 4$) show divergence in growth rate in the absence of inertia as one approaches the pure polymer melt ($\mu_r \to 0$) regime. Figures 5(a) and 5(b) show the effect of viscosity ratio (in the limit of $\mu_r \to 0$) on supported and freestanding viscoelastic liquid films respectively for $W = 10$. The divergence in the growth rate of supported viscoelastic liquid film can be seen from Figure 5(a). The corresponding variation of maximum growth of supported viscoelastic liquid film, with the viscosity ratio is shown Figure 5(c), which shows ω_m diverges as μ_r^{-1}. Even for freestanding viscoelastic liquid films, the decrease in viscosity ratio enhances the instability until a certain extent and a further decrease in viscosity ratio does not affect the instability as shown in Figure 5(b). We can see from Figure 5(b) that the dominant wavelength shifts towards shorter wavelengths with decrease in the viscosity ratio for freestanding viscoelastic liquid films, unlike supported viscoelastic liquid films for which the dominant wavelength remains unaffected. Inclusion of inertia in freestanding viscoelastic liquid films causes the maximum growth rate to remain bounded as shown in Figure 5(d) at very low values of viscosity ratio.

The variation of maximum growth rate with Weissenberg number, for different viscosity ratios as we approach the pure polymer melt regime, is depicted in Figures 6(a) and 6(b) for thin supported and freestanding viscoelastic liquid films respectively. Figure 6(a) clearly shows the di-

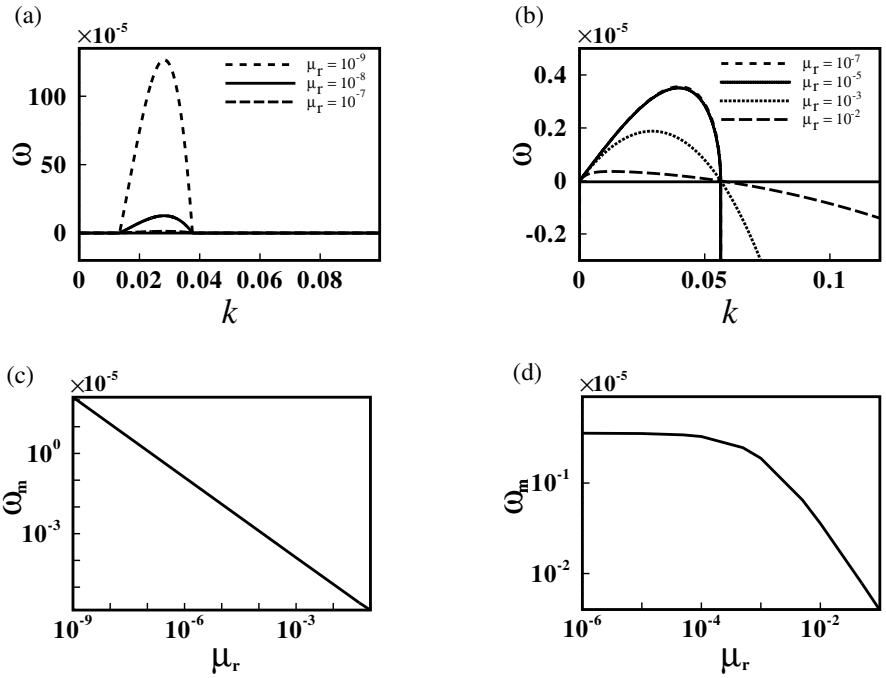

FIG. 5. Effect of viscosity ratio on the instability of thin supported and freestanding Jeffreys viscoelastic films in the limit $\mu_r \to 0$ and when $W > 4$. Plots (a) and (b) respectively show the ω vs k curves of thin supported and freestanding viscoelastic liquid films for different viscosity ratios. Plot (c) shows the divergence of the maximum growth rate of thin supported viscoelastic liquid films with viscosity ratio. Plot (d) shows that the maximum growth rate of a thin freestanding viscoelastic liquid film remains bounded and reaches a saturation value at very low values of μ_r. Weissenberg number ($W = 10$) is same in all the plots.

vergence of growth rate of supported viscoelastic liquid films (in the zero-inertia limit) at $W = 4$ for very low values of viscosity ratio. The presence of solvent contribution even in small quantity removes the divergence. Thus, thin supported viscoelastic liquid films with no solvent contribution in the zero inertia limit show divergence at $W = 4$. Unlike thin supported viscoelastic liquid films, Figure 6(b) shows that Weissenberg number does not significantly influence the maximum growth rate of thin freestanding viscoelastic liquid films and also that the decrease in viscosity ratio does not enhance the maximum growth rate beyond a certain extent.

In our discussion, thus far, inertia is retained for a thin freestanding Jeffreys viscoelastic film. Figure 7 compares the reuslts obtained for a Jeffreys viscoelastic freestanding film in the presence and absence of fluid inertia. Figure 7(a) shows ω vs k curves for an asymptotic case of Newtonian freestanding film (obtained when $W = 0$ and $\mu_r = 1$ in the Jeffreys model). Inertia is retained in curve 1 of this plot and neglected in curve 2. This result is in agreement with that of Sharma et al[42]. Figures 7(b) and 7(c) respectively show the ω vs k curves of a freestanding viscoelastic liquid film with and without inertia at different values of Weissenberg number. The viscosity ratio is taken as 10^{-6}. We can see from magnitudes of the maximum growth rate in these figures that neglecting

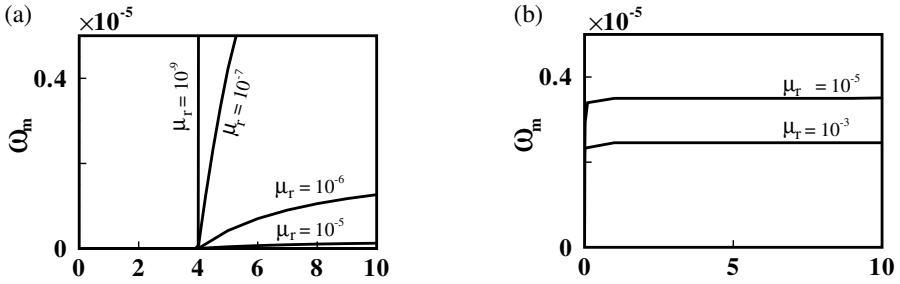

FIG. 6. Variation in the maximum growth rate with Weissenberg number (W) for different μ_r near pure polymer melt regime. Plot (a) refers to thin supported viscoelastic liquid film. Plot (b) refers to thin freestanding viscoelastic liquid film.

inertia leads to divergence even in thin freestanding viscoelastic liquid films. Figure 7(d) clearly shows the divergence of maximum growth rate for a thin freestanding viscoelastic liquid film as we approach pure polymer melt regime ($\mu_r \to 0$) when inertia is not retained.

D. Amplitude ratio and mode of deformation

Most previous studies on the instability of thin freestanding films presume a symmetric squeezing mode of deformation and employ the symmetry conditions at the centerline of the film as boundary conditions. In this article, LSA is carried out without imposing the mode of deformation a priori, thus independently perturbing both the free interfaces of the freestanding film. In order to ascertain the mode of instability, amplitude ratio (δ_r) for a thin freestanding film is evaluated for each rheological model, as given in Section IV. The value of δ_r turns out to be -1 in each case, for thin freestanding films, which shows that the instability mode is squeezing in nature and the magnitude of disturbances at both the interfaces are identical. As the configuration considered here is symmetric, unequal deformations do not occur at the interfaces.

VI. CONCLUSIONS

We have carried out a general linear stability analysis of thin freestanding films under the influence of attractive van der Waals forces for three different rheologies, viz. viscous film, zero-frequency viscoelastic solid film and Jeffreys viscoelastic liquid film. The influence of rheological parameters on the instability of these films has been studied in detail. The present study shows that GLSA results of a freestanding Newtonian film exactly match with the corresponding long-wave linear stability results from the literature[42]. The elasticity of solid in the thin freestanding films governs the onset of instability unlike the freestanding Newtonian films which are unconditionally unstable. Thin supported viscoelastic solid films[33] exhibit a finite wavenumber instability whereas thin freestanding viscoelastic solid films are unstable for longer wavelengths below the critical shear modulus. The elasticity of the solid has a stabilizing effect on the instability unlike in the case of Jeffreys fluid where viscoelasticity enhances the instability.

GLSA results of thin freestanding Jeffreys viscoelastic liquid film are compared with those of thin supported Jeffreys viscoelastic liquid film in the zero-inertia limit. Unlike supported viscoelastic liquid films, where both W and μ_r affect the instability, in a freestanding viscoelastic

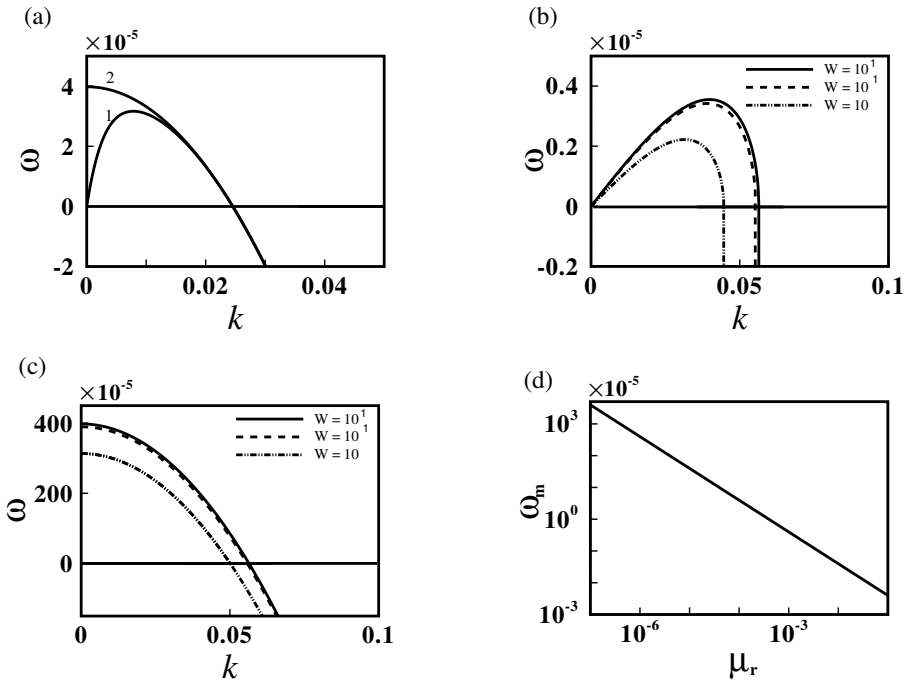

FIG. 7. Effect of inertia on the instability of thin freestanding Jeffreys viscoelastic films. Plot (a) shows the asymptotic case of a thin freestanding Newtonian film. Curves 1 and 2 refer to the films with and without inertia. Parameters in this plot are the same as used in Figure 2(a). Plots (b) and (c) show the ω vs k curves of thin freestanding Jeffreys viscoelastic films with and without inertia respectively at three different values of Weissenberg number (W). Viscosity ratio in these plots is kept constant at 10^{-6}. Plot (d) shows the variation in maximum growth rate with viscosity ratio in the absence of inertia. $W = 10$ in this plot.

liquid film, the instability is not significantly affected by W. In marked contrast to supported viscoelastic liquid films[31], in freestanding films with inertia, the maximum growth rate remains bounded and reaches saturation value independent of W, as $\mu_r \to 0$. The dominant length scale is not affected by rheological parameters in the case of supported viscoelastic liqid films, whereas in freestanding films, the dominant length scale shifts towards shorter wavelengths with decrease in μ_r. Neglecting inertia in thin freestanding viscoelastic liquid films, however, leads to a divergence of maximum growth rate, similar to supported viscoelastic liquid films. Thus, the present study shows that the instability of a thin freestanding Jeffreys viscoelastic liquid film is unaffected by the relaxation time, but is enhanced with decrease in the ratio of solvent to total viscosity; in the limit of viscosity ratio approaching zero, maximum growth rate remains bounded when inertia is retained, but diverges upon its omission. In general, the linear stability analysis shows that thin freestanding viscoelastic films exhibit faster dynamics than thin supported viscoelastic films. The most unstable mode for a thin freestanding film from our analysis is found to be a squeezing mode with equal amplitudes at both the interfaces for the symmetric configuration.

ACKNOWLEDGEMENTS

We thank Prof. Ashutosh Sharma for the valuable discussions. S.S. gratefully acknowledges Prof. Dipankar Bandyopadhyay for his valuable inputs.

DATA AVAILABILITY

The data that support the findings of this study are available from the corresponding author upon reasonable request.

REFERENCES

[1]K. Koch, B. Bhushan, and W. Barthlott, "Diversity of structure, morphology and wetting of plant surfaces," Soft Matter **4**, 1943–1963 (2008).
[2]K. Koch, B. Bhushan, Y. C. Jung, and W. Barthlott, "Fabrication of artificial lotus leaves and significance of hierarchical structure for superhydrophobicity and low adhesion," Soft Matter **5**, 1386–1393 (2009).
[3]Z. Wang, L. Zhu, W. Li, and H. Liu, "Bioinspired in situ growth of conversion films with underwater superoleophobicity and excellent self-cleaning performance," ACS Appl. Mater. Interfaces **5**, 10904–10911 (2013).
[4]H. A. Stone and S. Kim, "Microfluidics: Basic issues, applications, and challenges," AICHE J **47**, 1250–1254 (2001).
[5]G. Chen, G. T. McCandless, R. L. McCarley, and S. A. Soper, "Integration of large-area polymer nanopillar arrays into microfluidic devices using in situ polymerization cast molding," Lab Chip **7**, 1424–1427 (2007).
[6]T. N. Michael and L. T. Kimberly, "A batch fabricated biomimetic dry adhesive," Nanotechnology **16**, 1159 (2005).
[7]L. F. Boesel, C. Greiner, E. Arzt, and A. del Campo, "Gecko-inspired surfaces: A path to strong and reversible dry adhesives," Adv. Mater. **22**, 2125–2137 (2010).
[8]J. Ralston, "Thin films and froth flotation," Adv. Colloid Interface Sci. **19**, 1–26 (1983).
[9]B. Albijanic, O. Ozdemir, A. V. Nguyen, and D. Bradshaw, "A review of induction and attachment times of wetting thin films between air bubbles and particles and its relevance in the separation of particles by flotation," Adv. Colloid Interface Sci. **159**, 1–21 (2010).
[10]S. Chandran and G. Reiter, "Transient cooperative processes in dewetting polymer melts," Phys. Rev. Lett. **116**, 88301 (2016).
[11]F. Brochard-Wyart, P. G. de Gennes, H. Hervert, and C. Redon, "Wetting and slippage of polymer melts on semi-ideal surfaces," Langmuir **10**, 1566–1572 (1994).
[12]K. Kargupta, A. Sharma, and R. Khanna, "Instability, dynamics, and morphology of thin slipping films," Langmuir **20**, 244–253 (2004).
[13]M. Lessel, J. McGraw, O. Bäumchen, and K. Jacobs, "Nucleated dewetting in supported ultrathin liquid films with hydrodynamic slip," Soft Matter **13**, 4756–4760 (2017).
[14]D. Peschka, S. Haefner, L. Marquant, K. Jacobs, A. Münch, and B. Wagner, "Signatures of slip in dewetting polymer films," Proc. Natl. Acad. Sci. **116**, 9275–9284 (2019).
[15]P. Gutfreund, O. Bäumchen, R. Fetzer, D. van der Grinten, M. Maccarini, K. Jacobs, H. Zabel, and M. Wolff, "Solid surface structure affects liquid order at the polystyrene–self-assembled-monolayer interface," Phys. Rev. E **87**, 12306 (2013).
[16]S. Ma, X. Zhang, B. Yu, and F. Zhou, "Brushing up functional materials," NPG Asia Mater. **11**, 24 (2019).

[17]R. I. Saye and J. A. Sethian, "Multiscale modeling of membrane rearrangement, drainage, and rupture in evolving foams," Science **340**, 720 (2013).
[18]R. Aveyard and J. H. Clint, "Foam and thin film breakdown processes," Curr. Opin. Colloid Interface Sci. **1**, 764–770 (1996).
[19]A. Kabalnov and H. Wennerström, "Macroemulsion stability: the oriented wedge theory revisited," Langmuir **12**, 276–292 (1996).
[20]D. S. Dimitrov, "Dynamic interactions between approaching surfaces of biological interest," Progr. Surface Sci. **14**, 295–424 (1983).
[21]C. Maldarelli, R. K. Jain, I. B. Ivanov, and E. Ruckenstein, "Stability of symmetric and unsymmetric thin liquid films to short and long wavelength perturbations," J. Colloid Interface Sci. **78**, 118–143 (1980).
[22]B. V. Derjaguin, "The definition and magnitude of disjoining pressure and its role in the statics and dynamics of thin liquid films," Kolloid Zh. **17**, 207 (1955).
[23]M. B. Williams and S. H. Davis, "Nonlinear theory of film rupture," J. Colloid Interface Sci. **90**, 220–228 (1982).
[24]A. Sharma and E. Ruckenstein, "An analytical nonlinear theory of thin film rupture and its application to wetting films," J. Colloid Interface Sci. **113**, 456–479 (1986).
[25]C. J. V. Oss, M. K. Chaudhury, and R. J. Good, "Interfacial lifshitz-van der waals and polar interactions in macroscopic systems," Chem. Rev. **88**, 927–941 (1988).
[26]G. Reiter, "Unstable thin polymer films: rupture and dewetting processes," Langmuir **9**, 1344–1351 (1993).
[27]A. Sharma, "Relationship of thin film stability and morphology to macroscopic parameters of wetting in the apolar and polar systems," Langmuir **9**, 861–869 (1993).
[28]A. Oron, S. H. Davis, and S. G. Bankoff, "Long-scale evolution of thin liquid films," Rev. Mod. Phys. **69**, 931–980 (1997).
[29]R. Seemann, S. Herminghaus, and K. Jacobs, "Dewetting patterns and molecular forces: A reconciliation," Phys. Rev. Lett. **86**, 5534–5537 (2001).
[30]U. Thiele, M. G. Velarde, and K. Neuffer, "Dewetting: Film rupture by nucleation in the spinodal regime," Phys. Rev. Lett. **87**, 16104 (2001).
[31]G. Tomar, V. Shankar, S. K. Shukla, A. Sharma, and G. Biswas, "Instability and dynamics of thin viscoelastic liquid films," Eur. Phys. J. E **20**, 185–200 (2006).
[32]R. V. Craster and O. K. Matar, "Dynamics and stability of thin liquid films," Rev. Mod. Phys. **81**, 1131–1198 (2009).
[33]A. Patra, D. Bandyopadhyay, G. Tomar, A. Sharma, and G. Biswas, "Instability and dewetting of ultrathin solid viscoelastic films on homogeneous and heterogeneous substrates," J. Chem. Phys. **134**, 64705 (2011).
[34]R. Mukherjee and A. Sharma, "Instability, self-organization and pattern formation in thin soft films," Soft Matter **11**, 8717–8740 (2015).
[35]A. Vrij, "Possible mechanism for the spontaneous rupture of thin, free liquid films," Discuss. Faraday Soc. **42**, 23–33 (1966).
[36]A. Scheludko, "Thin liquid films," Adv. Colloid Interface Sci. **1**, 391 (1967).
[37]E. Ruckenstein and R. K. Jain, "Spontaneous rupture of thin liquid films," J. Chem. Soc. Faraday Tras. II **70**, 132–147 (1974).
[38]M. Prévost and D. Gallez, "Nonlinear rupture of thin free liquid films," J. Chem. Phys. **84**, 4043–4048 (1986).
[39]A. Sharma and E. Ruckenstein, "Stability, critical thickness, and the time of rupture of thinning foam and emulsion films," Langmuir **3**, 760–768 (1987).

[40]T. Erneux and S. H. Davis, "Nonlinear rupture of free films," Phys. Fluids A **5**, 1117–1122 (1993).
[41]A. D. Wit, D. Gallez, and C. I. Christov, "Nonlinear evolution equations for thin liquid films with insoluble surfactants," Phys. Fluids **6**, 3256–3266 (1994).
[42]A. Sharma, C. S. Kishore, S. Salaniwal, and E. Ruckenstein, "Nonlinear stability and rupture of ultrathin free films," Phys. Fluids **7**, 1832–1840 (1995).
[43]O. K. Matar, "Nonlinear evolution of thin free viscous films in the presence of soluble surfactant," Phys. Fluids **14**, 4216–4234 (2002).
[44]M. S. Bazzi and M. S. Carvalho, "Effect of viscoelasticity on liquid sheet rupture," J. Non-Newtonian Fluid Mech. **264**, 107–116 (2019).
[45]Y. L. Zhang, O. K. Matar, and R. V. Craster, "Analysis of tear film rupture: effect of non-newtonian rheology," J. Colloid Interface Sci. **262**, 130–148 (2003).
[46]M. Rauscher, A. Münch, B. Wagner, and R. Blossey, "A thin-film equation for viscoelastic liquids of jeffreys type," Eur. Phys. J. E **17**, 373–379 (2005).
[47]J. Sarkar and A. Sharma, "A unified theory of instabilities in viscoelastic thin films: From wetting to confined films, from viscous to elastic films, and from short to long waves," Langmuir **26**, 8464–8473 (2010).
[48]V. Barra, S. Afkhami, and L. Kondic, "Interfacial dynamics of thin viscoelastic films and drops," J. Non-Newtonian Fluid Mech. **237**, 26–38 (2016).
[49]R. Larson, *Structure and Rheology of Complex Fluids* (Oxford, 1998).
[50]D. Bandyopadhyay, A. Sharma, and V. Shankar, "Instabilities and pattern miniaturization in confined and free elastic-viscous bilayers," J. Chem. Phys. **128**, 154909 (2008).